REGENERATION OF MATERIALS BY ELECTRON BEAM MELTING AND REFINING OF REFRACTORY METALS AND ALLOYS IN VACUUM

Project DO 02/200 financed by the Bulgarian National Science Fund
at the Ministry of Education, Youth and Science

K Vutova, V Donchev, V Vassileva, E Koleva and G Mladenov
Emil Djakov Institute of Electronics, Bulgarian Academy of Sciences,
72 Tsarigradsko Chaussee, 1784 Sofia, Bulgaria

The relevance of the problem of fabricating new materials by recycling of scrap by electron beam melting and refining (EBMR) of refractory and reactive metals and alloys is justified by the environmental friendliness of the method and the fact that it enables one to obtain materials with new and improved chemical composition, structure, and properties. The materials thus processed find numerous applications in the nuclear power industry, medicine, space engineering, automotive industry, tool engineering, etc. A sharp increase in the activities on designing, implementating and operating equipment for refractory and reactive metals and alloys by EBMR has taken place in recent years. Large manufacturers in countries such as the U.S., India, China, Russia, France, Germany, have shown particular interest in developing such technologies.

Despite the rapid development in the field of EBMR, many unsolved problems still remain. The study of mechanisms and relationships of macroscopic heat and mass transfer during heating a free liquid surface by an intensive energy flux is a fundamental problem. Improving the energy efficiency is crucial in optimizing the technologies and reducing the price of the pure metals obtained. This requires detailed studies of the thermal processes taking place in the zone of beam-material interaction, thorough knowledge of the processes and factors limiting the geometry of the molten pool, and precise evaluation of the temperature distribution and behavior of the metals and their compounds in the refining process. The successful application and optimization of EBMR depend also on the adequate mathematical modeling of the processes involved; this will assist one in studying the influence of the large number of technological parameters and the various limiting factors. The research tasks performed and some of the main results obtained in 2012 in view of achieving the main objective of the present project are:

A time-dependent heat model for simulation of the heat transfer in metal ingots solidified in a water-cooled crucible during EBRM (figure 1) that is a continuation and extension of our quasi-steady-state heat model [1,2,3] was proposed and developed [4,5]. The temperature distribution along the cast ingot (figure 1) was described by the heat equation in cylindrical coordinates with angle symmetry:

$$\frac{1}{r}\frac{\partial}{\partial r}\left(r\frac{\partial T}{\partial r}\right)+\frac{\partial^2 T}{\partial z^2}+\frac{V}{\alpha}\frac{\partial T}{\partial z}=\frac{\rho C_p}{\lambda}\frac{\partial T}{\partial t} \quad (1)$$

where $T(r, z, t)$ denotes the temperature at heating time t at points with height z and polar distance r; ρ is the density of the metal; the last term in the left-hand side of equation (1) describes the casting process, i.e., the heat added by the molten metal poured (from the raw material being melted) into the crucible (figure 1), which is given by the heat energy transfer from the material moving with velocity V along the z-axis; a is the thermal diffusivity.

By assuming three mechanisms of heat transfer through the different boundaries (figure 1), i.e., three types of thermal contact

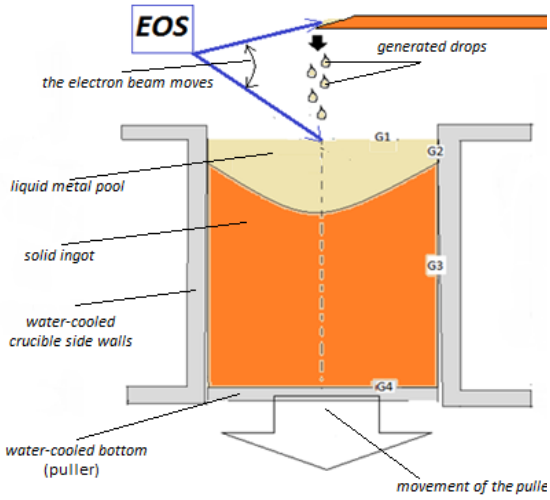

Figure 1. Schematic of the drip EBMR method. G1- the top surface of the ingot; G2 – the molten ingot/crucible wall interface; G3- the ingot/vacuum interface; G4- the ingot/puller interface.

interfaces, namely, areas with ideal thermal contact; areas with Newton's type of heat transfer and areas where the radiation losses predominate, the corresponding boundary conditions were formulated taking into account the radiative and vaporization losses. A modified Pismen-Rekford method was developed and applied to calculating the temperature fields in the cast ingot. The numerical scheme developed is absolutely stable and implicit in terms of the heating time. The implicit nature of the scheme was overcome by applying the Thomas method for solving three-diagonal linear systems. The temperature dependencies of the thermal conductivity λ and the specific heat capacity C_p for each metal investigated were estimated using experimental data [6,7]. The corresponding functions obtained (on T) were included in the model.

The model proposed was modified and applied also to the simulation of the thermal processes in the feeding rod (figure 1). A corresponding computer program was developed and used to study the thermal processes during e-beam melting and recycling of metals (figure 1). The model was validated and numerical experiments were performed for wide ranges of variation of the values of the parameters involved in EBMR of tantalum, titanium, copper and aluminum. Important data were obtained about the heat fluxes through the boundaries, the geometry of the molten pool, the temperature distributions in vertical and/or horizontal cross-sections of the cylindrical metal samples, and recommendations were given concerning the choice of proper regime conditions in order to optimize the EBMR process.

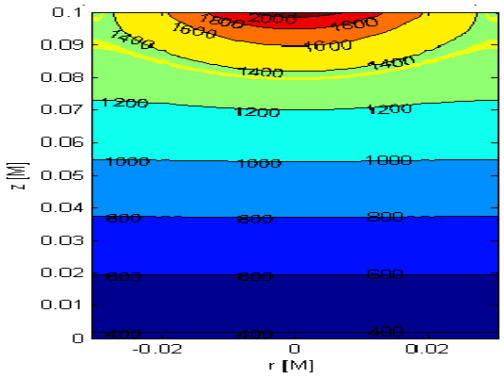

Figure 2. Temperature distribution in a vertical cross-section of a Cu ingot ($2R$ = 60 mm, H = 100 mm). The yellow line (T_{melt} = 1356 K) is the liquid/solid boundary (crystallization front). Beam power P = 20 kW, beam radius r_b = 12 mm, t = 10 min, V = 0 mm/min.

The temperature field calculated in a vertical cross-section of the copper ingot at the 10th minute of the heating is shown in figure 2. The yellow line is the temperature contour corresponding to T_{melt} = 1356 K, i.e., the liquid/solid boundary. The crystallization front (the liquid/solid boundary) shape is directly connected with the quality of the casting metal ingot – a flat crystallization front permits the formation of dendrite structures parallel to the ingot axis, as well as uniform impurity displacement toward the block top surface. The simulation results showed that the lowest casting velocity value, for which the molten metal pool starts contacting with the crucible side wall (G2), is 5 mm/min (table 1). The results presented in figure 3 demonstrate the non-steady-state nature of the process at the G2 interface (the interface molten

Table 1. Dynamics of the contact molten metal pool/cooled side wall of the crucible (G2) for EBMR of Cu.

V, mm/min	First moment of contact at G2, s	Total time of contact at G2, s
5	650	1
6	500	5
7	350	21
8	300	43
9	250	74
10	220	86

ingot/crucible wall – figure1) – alternation of contact molten pool/cooled side crucible wall and withdrawal of the ingot surface. The duration of the contact at G2 is only 5 s from a total of 500 s for $V = 6$ mm/min and only 86 s of 220 s for $V = 10$ mm/min (table 1, figure 3). The liquid pool depth for $V = 5 \div 10$ mm/min is constant and is about 11 mm. For the higher values of casting velocities ($V = 9$, 10 mm/min), the pool dimensions become stable (figure 3), which is a condition for more efficient refining processes.

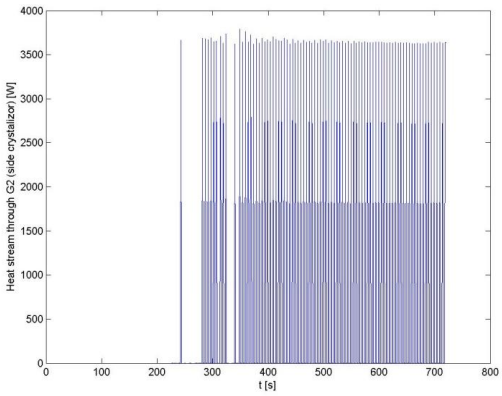

Figure 3. Dynamics of the thermal losses through the G2 boundary. Each jump corresponds to an actual contact molten pool/crucible wall (G2 interface) for 1 sec, $V = 10$ mm/min.

The non-steady-state heat model was also applied to EBMR of the refractory metal tantalum for casting velocities $V = 0$, 3, 6 and 9 mm/min and different ingot heights H in order to study the pool geometry changes and the ingot quality. The heating time t is up to 10 min and the beam radius r_b is 16 mm. The results presented in figure 4 show that the casting velocity V influences strongly the volume of the molten pool V_m.

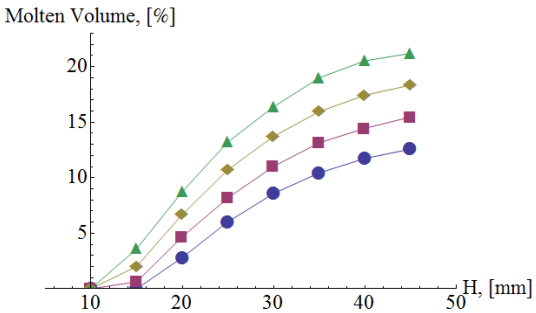

Figure 4. Variation of the molten volume $V_m/V_{ingot} \times 100$ (in %) in Ta at the 10th minute and for $P = 24$ kW vs. the ingot height H for:
$V = 9$ mm/min – triangles;
$V = 6$ mm/min – diamonds;
$V = 3$ mm/min – squares;
$V = 0$ mm/min – circles.

The results show that the liquid pool depth h_m stabilizes after five minutes heating and an almost fully molten top ingot surface is achieved for $H = 40$ and 45 mm and $V = 6$ and 9 mm/min (table 2). As V increases, a fully liquid top surface of the ingot is observed earlier (for a shorter heating time), e.g., for $H = 45$ mm – at the 230th s for $V = 9$ mm/min, and at the 500th s for $V = 3$ mm/min (table 2). This is seen even for shorter ingots. Furthermore, earlier stabilization of the liquid pool depth is achieved when the casting velocity is increased; this ensures better refining condition.

A series of experiments implementing different technological regimes and methods were performed in our laboratory using the ELIT 60 equipment for EBMR of tantalum, titanium, copper, hafnium, aluminum, alloy steel, etc. The liquid pool shape variation (experimental and simulation data) in titanium samples vs. the refining time is shown in figure 5 for heating e-beam power of 2.4 kW, $r_b = 12$ mm and $V = 0$ mm/min. A good agreement is seen between the calculated and the experimentally obtained shapes of the crystallization front.

Table 2. Molten pool geometry data in Ta and time for stabilization of the liquid pool dimensions for different ingot heights *H* and casting velocities *V*.

H, mm	*V*, mm/min	3	6	9
35	pool diameter/time for stable pool	41 mm/400 s	45 mm/400 s	50 mm/350 s
	pool depth/ time for stable pool	6.5 mm/430 s	9 mm/420 s	10 mm/400 s
40	pool diameter/time for stable pool	45 mm/450 s	50 mm/380 s	50 mm/260 s
	pool depth/ time for stable pool	9 mm/400 s	10 mm/400 s	10.7 mm/330 s
45	pool diameter/time for stable pool	50 mm/500 s	50 mm/300 s	50 mm/230 s
	pool depth/ time for stable pool	10 mm/400 s	11 mm/400 s	12 mm/340 s

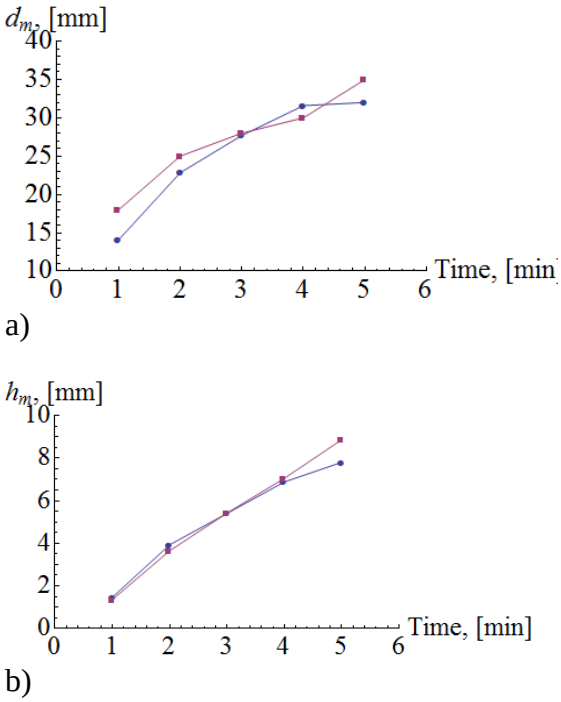

Figure 5. Dependence of the molten pool dimensions: (a) pool diameter d_m and (b) pool depth h_m on the heating time during EBMR of Ti, where (●) represents simulation results and (■), experimental data.

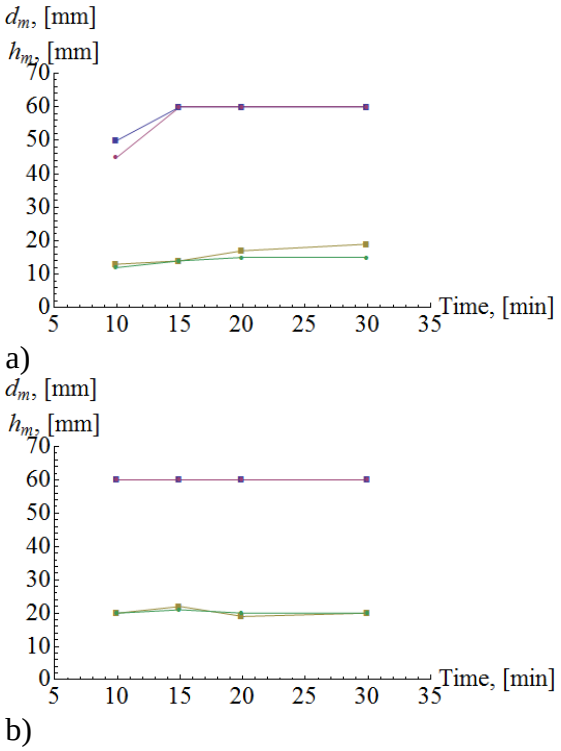

Figure 6. Comparison between experimental and simulation data for the diameter d_m (upper curves) and the depth h_m (lower curves) of the molten pool in Cu during EBMR by: (a) 10 kW beam power; (b) 15 kW beam power. (●) represents simulation results and (■), experimental data.

Experimental data for liquid pool dimensions – pool diameter d_m (upper curves, figure 6) and pool depth h_m (lower curves, figure 6) obtained for EBMR of copper ingots ($2R$ = 60 mm, H = 50 mm) with beam powers of 10 kW and 15 kW are compared with calculated data and are presented in figure 6. A good agreement is seen, namely, less than 10 % mean deviation value.

The crystallization front shape obtained experimentally and the calculated liquid/solid boundary are given on the

metallographic photograph (figure 7) of a tantalum ingot cross-section after e-beam melting with beam power of 27 kW; a reasonable agreement can be seen. The temperature fields as calculated numerically and measured experimentally agree well, too – figure 8.

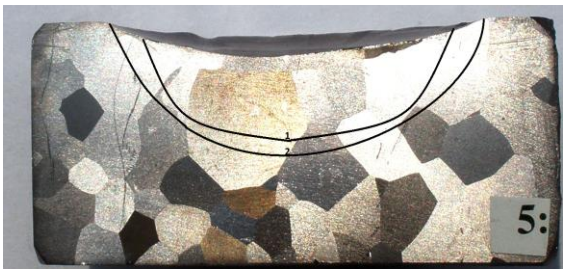

Figure 7. Comparison between the calculated (curve 1) and experimentally observed (curve 2) liquid/solid boundaries on a metallographic photograph of a Ta ingot.

Using experimental data for EBMR of copper, regression models for residual impurities concentration (after EBMR) were considered. The models obtained for the impurities studied (Pb, Sb, Ni, Zn, As, Sn, Bi) and the corresponding determination coefficients are given in table 3. The variation of the concentration of the impurities vs. the e-beam power and the refining time were studied and optimal data for the concentration of the residual impurities were obtained.

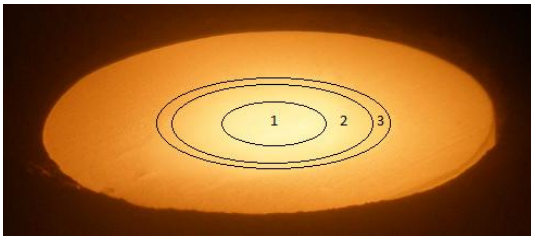

Figure 8-a. Temperature level lines on the top sample surface at the first minutes of e-beam heating of Ta with a 6-kW e-beam. 1 - [975 K - 1025 K], 2 - [850 K - 975 K], 3 - [880 K - 850 K].

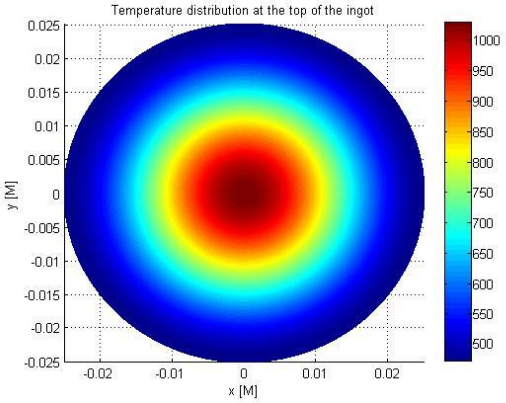

Figure 8-b. Numerically calculated 2D temperature distribution on the top surface of the ingot at t ≈ 60 s.

A graphical user interface (GUI) for studying the EBMR of copper was developed based on the regression models considered. For concrete values of the refining time and the beam power, the residual concentrations of the impurities

Table 3. Regression models and determination coefficients.

	Model	R^2	R^2adj	R^2pred
As	$y_1=0.772-0.002x_1-0.031x_2-1.702x_1^2-0.212x_1^3+1.751x_1^4+0.072x_1^3x_2$	0.77131	0.70271	0.61120
Bi	$y_2=0.058-0.001x_1-0.012x_2-0.587x_1^2-0.071x_1^3+0.603x_1^4+0.028x_1^3x_2$	0.73416	0.65441	0.55322
Pb	$y_3=0.743+0.046x_1-0.081x_2-3.185x_1^2-0.598x_1^3+3.440x_1^4+0.175x_1^3x_2$	0.87303	0.83494	0.76498
Sb	$y_4=0.949+0.013x_1-0.065x_2-2.470x_1^2-0.362x_1^3+2.587x_1^4+0.142x_1^3x_2$	0.81287	0.75673	0.65760
Ni	$y_5=0.959-0.387x_1-0.141x_2-3.161x_1^2+3.273x_1^4$	0.74330	0.69663	0.61149

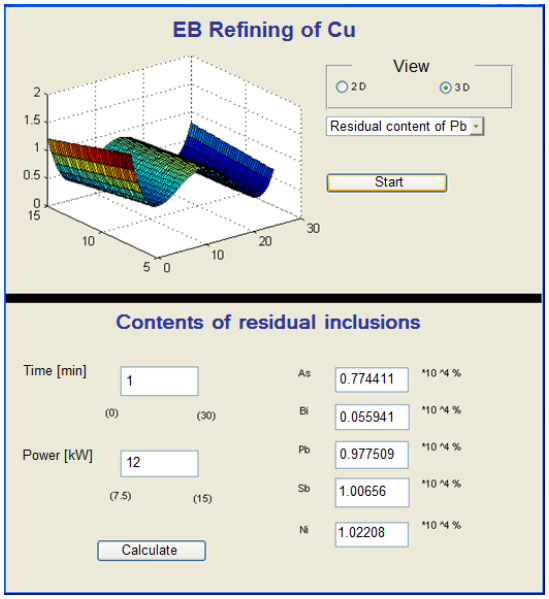

Figure 9. Screenshot of GUI showing: (i) 3D dependence of the Pb concentration on the beam power and refining time and (ii) residual impurities' concentration for EBMR of copper for 12 kW beam power and 1 min refining.

are calculated in the lower part (figure 9), while, in the upper part, a 2D or 3D graphical image can be drawn presenting the concentration dependence of the chosen impurity on the beam power and on the refining time (figure 9). Figure 9 presents an example for 1-min refining time and 12-kW e-beam power for EBMR of copper and a 3D visualization of the Pb impurity concentration variation. The GUI developed allows one to select more easily the regime parameters thus achieving better process optimization.

On the basis of the experimental and theoretical studies performed, data and dependencies of practical importance were obtained and recommendations were formulated for choosing the proper process conditions. The results are important and useful in view of studying, controlling and optimizing the quality and purity of the new materials obtained by EBMR.

Agreements were signed between IE-BAS and two Bulgarian companies for joint research and development of technologies for EBMR of refractory metals and alloys, as well as for recycling of precious metals and alloys. Studying the processes involved in EBMR and developing better technologies and equipment for obtaining new materials by recycling waste products of refractory, reactive and other metals and alloys using EBMR form a good basis for technological transfer and for specialized industrial applications of the research results obtained.

References

[1] Vutova K, Vassileva V and Mladenov G 1997 *Vacuum* **48**/2 143-8

[2] Vutova K, Koleva E and Mladenov G 2011 *IREME – Special Issue on Heat Transfer* **5** 257-65

[3] Vutova K, Donchev V, Vasileva V and Mladenov G 2012 *Supplemental Proceedings: Materials Processing and Interfaces* (TMS Wiley USA) **1** 125-32

[4] Vutova K and Donchev V 2012 Proc. 10th Int. Conf. EBT'12 Varna *J. Electronics and Electrical Engin.* **47**/5-6 273-9

[5] Vutova K, Donchev V, Vassileva V, Amalnerkar D P, Munirathnam N and Prakash T 2013 *EPD Congress 2013 volume* (TMS Wiley USA) accepted for publication

[6] Samsonov G 1965 *Chemo-physical properties of elements* (Kiev: Naukova Dumka Publ. House) 202-27 (in Russian)

[7] Gurevich S M 1982 *Metallurgy and technology of refractory metals and alloys welding* (Kiev: Naukova Dumka Publ. House) 13 (in Russian)